Structural model of amorphous arsenic sulfide

C. J. Brabec
Department of Physics, North Carolina State University, Raleigh, North Carolina 27695-8202
(Received 19 June 1990; revised manuscript received 22 July 1991)

Modeling studies of amorphous (*a*-) semiconductors have recently enjoyed renewed interest because of increasing access to computing power and experimental developments that have revealed more information about local atomic structure. Amorphous arsenic sulfide (*a*-As_2S_3) is a paradigm of an amorphous material that exhibits structural bistability, and therefore is a prime candidate for investigations of models. Previous studies of this material have suggested that *a*-As_2S_3 consists of either helical or planar structures or bridged parallel chains. Experimental investigations alone have not led to a resolution of which of these proposed structures most accurately represents the actual material. We have built a model of *a*-As_2S_3 that consists of 1790 atoms and agrees relatively well with all experimental studies of the material that can be directly compared with a computer model. These include the density, the (infrared) vibrational properties, the radial distribution function, pair distribution functions, neutron (and x-ray) diffraction spectra, and elastic moduli. By studying the dihedral-angle relationships in the model, it can be determined that *a*-As_2S_3 consists of randomly oriented segments of helical chains. The model does not contain planar structures or bridged parallel chains.

I. INTRODUCTION

Studies of amorphous (*a*-) semiconductors have recently enjoyed renewed interest due to increasing access to computing power and experimental developments that have revealed more information about local atomic structure. Structure and structural changes in amorphous materials represent a family of interesting problems that lend themselves to modeling studies. In an argument based on balancing constraints with degrees of freedom, it has been suggested[1] that the optimum coordination number for a material to exhibit a structural bistability is 2.44. The coordination number of *a*-As_2S_3 is 2.4, so it is not surprising that *a*-As_2S_3 is considered by many to represent a paradigm of an amorphous multistable material and as such, a prime candidate for modeling investigations. Investigations of materials from the family of chalcogen-containing glasses are also driven somewhat because of interest in their potential technological applications in such fields as imaging and information storage. Despite these technological and fundamental interests, the modifications that lie at the heart of the structural bistability in *a*-As_2S_3 and materials like it are not well understood. It is knowledge of the structure of *a*-As_2S_3 and the mechanism behind its structural bistability that represents the ultimate goals of this research.

The bistability of *a*-As_2S_3 manifests itself in a reversible photodarkening effect. In its annealed state, *a*-As_2S_3 is a yellow glass. It can be changed to a photodarkened state by illumination, which causes the glass to turn redder in color. This change is reversible. Heating of the material to a temperature near its glass transition temperature causes it revert to the annealed state.

Theoretical studies of the structure of materials can often be aided through the use of models. The proper use of modeling can lead to insight into the structure of the actual material, but one must be careful in interpreting modeling results. In particular, several caveats must be kept in mind. First, one must be careful to check any model against all experimental data that are available for which a meaningful check can be made. Then, once one is assured that the constructed model is consistent with existing data on the actual material, one must be careful in interpreting the value of one's model. This is because agreement with experiments performed on the real material is necessary but not sufficient condition that a model truly mimics the actual material structure. Thus, modeling is often used to rule out unambiguously structures that do not pass the experimental check, but it alone may not be used to identify the structure of the real material absolutely.

Balancing these cautions, the modeling of amorphous structures has several strengths. For one, modeling can lead to further experiments that might not have been thought of in the absence of modeling. Another strength lies in the ability to identify, in models, elements of intermediate-range order (IRO) that are elusive, if not undetectable, in the actual material. These two strengths of modeling are particularly important in the present study. Insofar as it is changes in intermediate range order that lead to the interesting photostructural modifications observed in *a*-As_2S_3, an accurate model of these intermediate range modifications can suggest mechanisms which may be responsible for the observed effects. Such proposed mechanisms can then lead experimentalists to laboratory checks of these mechanisms and ultimately to a better understanding of the real material.

The modeling of the atomic structure of amorphous materials has a history almost as long as the study of the materials themselves.[2] Current interest in modeling has been rekindled for two principal reasons. First, experimental probes of intermediate-range order have become

availible. The clearest example of these involves the x-ray-absorption-spectroscopy data which allow for the determination of pair-distribution functions in an amorphous material.[3] The atom specificity involved with this spectroscopy coupled with an ability to use phase information in the transformation of data[4] make intermediate-range-order information available that simply was not accessible in the past. A second reason for renewed interest in this type of modeling involves the increased availability of computer power. Increased power has allowed for construction of larger models (with a concomitant smaller fraction of surface atoms), more realistic atomic potentials, and more complete computer relaxation.

Remaining aware of the limitations inherent in the modeling of amorphous materials, while at the same time being encouraged by additional experimental results and greated available computer power, the present study was undertaken. In the following we first describe current knowledge of the basic structure of a-As_2S_3 and then introduce the concept of intermediate-range order, stressing experimental probes of structure at this level. We then review briefly previous models of a-As_2S_3 and describe our own model-building technique. Finally we compare our model with experimental data and draw possible conclusions about the structure of the real material based on our modeling results.

II. STRUCTURE OF As_2S_3 AND INTERMEDIATE-RANGE ORDER

To understand the ordering of a-As_2S_3 it is instructive to first examine the atomic arrangements in its crystalline (c-) counterpart, orpiment, that is, c-As_2S_3. In orpiment AsS_3 pyramidal units form helices which cross link into 12-membered rings.[5] Adjacent rings are covalently bonded into planes, and these planes are principally weakly van de Waals bonded to form the anisotropic solid. Descriptions of the structure of a-As_2S_3 usually begin with an AsS_3 pyramidal unit. The argument for the existence of such a unit based on vibrational data, and there is general agreement that these pyramids provide a convenient framework for discussions of the amorphous As_2S_3 network.

For higher-order structures in the amorphous material, no such consensus exists. By careful examination of the symmetries of vibrations in the crystal and the infrared and Raman spectra of the glass,[6] larger structures have been described in terms of -As-S-As-S-As- chains that link into planar structures. Appeal to such chains appears in other work as well.[7] With the addition of nuclear-quadrupole-resonance techniques,[8] coherent relationships between planes have been proposed. Some groups[9] have discussed large structural configurations in terms of bridged parallel chains which center on 12-member rings of alternating As and S atoms. A number of other research teams[10] have pursued this notion, as well as that of other clusters[11] which may be stable constituents of the disordered network.

These studies and others like them have driven discussions of the structure of these materials to consider the notion of *intermediate-range* order. To establish a framework for our discussion we first must recognize what we mean by *short-range* order. Clearly, the atomic arrangements that include definitions of an atom's neighbors and the bond lengths and angles joining neighbors falls into the regime of short-range order. If one includes the notion of higher-order correlations and local symmetries in this regime, then the notion of dihedral angle relationships (four-body correlations) must also be considered. We prefer inclusion of all of these in the definition since this naturally places the notion of local-site symmetry squarely in the realm of short-range order. We next suggest that materials for which microcrystallinity is experimentally observable (using, for example, x-ray or electron diffraction of Raman spectroscopy) are said to possess *long-range* order. Particle correlations extending to larger numbers of atoms than those included in short-range order but which do not manifest themselves in the long-range order signature are said to encompass the realm of *intermediate-range order.*

Our choice of such a definition is of course arbitrary. It does provide, however, a criterion that is not material dependent and has a framework with a physical basis. Other perfectly acceptable definitions include the suggestion of Elliott[12] that descriptions of dihedral angle relationships are the smallest units of intermediate-range order. Some researchers prefer to arbitrarily set the line of demarcation between short- and intermediate-range order at a particular distance (say 10 Å) or a particular coordination sphere.[13] Finally, some appeal mostly to experimental responses of systems.[14] This implies that the definition of intermediate-range order lies in, for example, spectral features of low-k x-ray spectra or in low-frequency Raman spectra. We have chosen the definition based on dihedral angle relationships and local symmetries because they lie at the heart of the problems we are investigating.

Experimental determination of intermediate range order in amorphous solids is difficult for two reasons. First, the lack of symmetries inherent in the amorphous state make symmetry-dependent characterization techniques (e.g., ir spectroscopy) problematic. Second, even if intermediate range order structures exist, the disorder broadening in many experimental measures of order can cause any signature of existing intermediate range structures to be masked by a broad distribution involving all intermediate range orientations.

As mentioned at the start of this section, the structure of a-As_2S_3 can be most easily discussed once the structure of c-As_2S_3 or orpiment, is understood. In orpiment, the linked AsS_3 pyramids which form the crystalline state can be seen as the building blocks of the helical chains in Fig. 1(a). The helical chains connect together across weaker-bonded bridging sulfur atoms to form layers. The layers alternate and are weakly bonded together with van der Waals forces. The entire multilayered structure consisting of bridged chains describes the crystalline state of As_2S_3 [Fig. 1(b)]. The study of IRO of a-As_2S_3 is principally a question of what degree of the order seen in the crystalline state (AsS_3 pyramids; pyramids linked into As-S-As-S-As-S chains; chains held together with bridg-

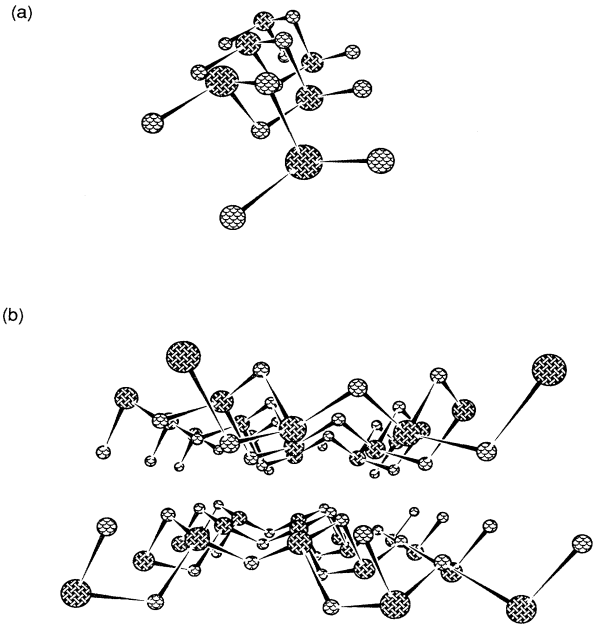

FIG. 1. (a) A helical chain of a-As_2S_3 and (b) crystalline As_2S_3 showing the formation of layers from the helical chains.

ing S atoms; or alternate layers of bridged parallel chains) exists in the amorphous material. As mentioned above, previous studies have suggested that the intermediate-range order in a-As_2S_3 takes the form of either layers, helices or bridged parallel chains. The importance of understanding the IRO in a-As_2S_3 is underscored by the fact that it has been previously determined that there is a relationship between the intermediate-range order of a-As_2S_3 and the photodarkening effect.[3] Through the present modeling studies, some possible forms of this IRO is identified, and the relationship between this intermediate-range order and the photodarkening effect is investigated.

Experiments have made it possible to determine some of the basic structural properties of a-As_2S_3 such as bond lengths, bond angles, density, and bulk modulus.[15,16] Other experiments have suggested more complex structural ordering of a-As_2S_3. These include x-ray and neutron scattering experiments. Lucovsky *et al.*[15] studied the vibrational aspects of a-As_2S_3. To interpret their data, they used a valence force field model employing bond lengths and bond angles. Using this model, they were able to determine the force constants associated with bond length and bond angle deviations. They also suggested that an AsS_3 pyramid constituted a basic building block of a-As_2S_3.

Yang *et al.*[3] studied a-As_2S_3 through extended x-ray absorption fine structure (EXAFS) experiments made at the arsenic absorption edge. They determined the arsenic structural distribution functions. These functions describe the radial distance between an arsenic atom and the atoms near it out to the third nearest neighbor. They suggested that the photodarkening effect related to the twisting of two joined AsS_3 pyramids and the expansion of the bond angle on the common sulfur atom.

III. MODELS OF AMORPHOUS STRUCTURES

A conceptually straightforward way of modeling amorphous structures involves the construction of mechanical (or stick-and-ball) models.[8] Such stick-and-ball models suffer in that they consider only the effects of bond lengths and bond angles on formation of the long-range structure. These models are also subject to gravitational sagging which displaces the atoms from their equilibrium positions. To avoid these problems, a stick-and-ball model can be relaxed in the computer after it has been built.[17] This relaxation process involves moving the atoms in the model to their minimum-energy positions. This removes effects of sagging on the model, and if an accurate interatomic potential can be developed, it allows the introduction of higher-order energy considerations beyond bond lengths and angles.

A variation of the relaxation method can also be used to create models. This substitution method uses models of one type of material and relaxes it with different types of atoms or with more atoms added in between.[18] This method has the advantage of allowing one to exploit extant models of relatively simple materials (e.g., a-As) to model more complicated structures (e.g., a-As_2S_3). This method is unrealistic, however, in that the structures present in the simpler starting material are imposed onto a physically different material.

There are other problems associated with stick-and-ball models that computer relaxation cannot resolve. The structure of a stick-and-ball model is limited to how the modeler builds it. Any preconceived notions the builder may have will be introduced to the model as biased structure. A model builder with no knowledge of the material being studied may still use a preferred structure throughout the model. One way to overcome modeler-dependent biases is through construction entirely using a computer. Computer-based modeling can follow a number of tacks, examples of which are discussed in the literature.[19–24]

A. Previous models of a-As_2S_3

Rechtin *et al.* produced a model of a-As_2S_3 containing 100 atoms.[21] This model began with a random cluster of atoms which was then relaxed using a Monte Carlo method such that it fit a given experimental radial distribution function. The Monte Carlo method involves randomly moving atoms and determining the energy change associated with the move. If the energy is lowered by the change, the move is retained. If the energy is higher, the move is retained with a probability $\exp(-dE/kT)$, where dE is the energy increase associated with the move, k is Boltzmann's constant, and T is temperature. Periodic boundary conditions are employed to avoid problems with finite sample size. This model shows very good agreement with the experimental radial distribution func-

tion, as would be expected, but is somewhat unrealistic in that it has a large number of internal dangling bonds which are known to be absent in the real material. Furthermore, no claims as to the intermediate-range order in the model are made.

Fujiwara *et al.*[19] produced models in a different way. They begin with a random close-packed structure of atoms which is relaxed using an atomic potential which involves bond lengths and bond angles only. The relaxation is achieved by determining the direction of the net force on an atom and moving that atom in that direction. Completion of the model was accomplished through iterative reformation of the bonds between atoms and subsequent relaxation. The results show good agreement with the experimental radial distribution function, and the model shows evidence for two-dimensional (planar) structures. This model is questionable, however, since it contains a large percentage of internal dangling bonds, which are known not to exist in the real material.

Fowler and Elliott[18] created models of a-As_2S_3 by a substitution method. Although this model agrees well with the experimental radial distribution function and x-ray diffraction results, a bias is built in since the model is based on a structure known to be different from the modeled material. Through careful study of how this model re-creates the first sharp diffraction peak (a feature of the x-ray diffraction spectrum), Fowler and Elliott concluded that their models could accurately model the x-ray diffraction without resorting to layers or bridged parallel chains. Thus they concluded that these structures were unlikely in a-As_2S_3.

Pfeiffer and co-workers used the relaxed stick-and-ball method to build several models.[7] To perform the relaxation, an atomic potential consisting of bond-stretching and bond-bending terms similar to those used by Fujiwara was employed. Also included were two terms that relate to the interaction between sulfur atom pairs. Each sulfur atom has two electrons which are not used in bonding. These lone-pair electrons can be modeled as a quadrupole of charge on each sulfur atom. The interaction of these quadrupoles form the basis for the other terms in the potential. These early models show reasonable agreement with the experimental radial distribution function and with x-ray diffraction experiments. The models do not have internal dangling bonds, but they are relatively small so they do suffer from finite size and surface problems. The models also show evidence for the existence of helical forms of intermediate-range order. This could, however, be a product of the initial bias inherent in hand-built models.

B. Building the model

The present model was constructed entirely using the computer, but the process used to build it was derived from the relaxed hand-built method. In the method chosen, the computer takes the part of the experimenter in randomly adding atoms to the growing model. The program is constrained always to add additional atoms to the atom with unfulfilled bonds that is nearest to the center of the existing model. In this way, the program avoids leaving dangling bonds, except—of course—on the surface of the growing model. The building algorithm furthermore only allows bonds between heteropolar atoms (As-S). Experimental evidence suggest that this configuration is preferred over homopolar (As-As or S-S) bonds.

The program proceeds by adding atoms and relaxing them into place. The relaxation process involves the use of the four-term potential suggested in our previous work:[7]

$$U = U_{\text{stretch}} + U_{\text{bend}} + U_{LP\text{-cross}} + U_{LP\text{-point}} \ . \tag{1}$$

Correcting potentials are used to accommodate interatomic bonding, to monitor the density, and to avoid the development of "bad pairs," which are atoms that are not bonded together but are closer together than one bond length. The building process is explained in detail in Appendix A.

The first two terms of the potential derive from the valence force field model of Lucovsky *et al.*[15] The first term is an harmonic potential based on the bond length between two bonded atoms. The form of this term is

$$U_{\text{stretch}} = (\tfrac{1}{2})\alpha(L - L_0)^2 \ , \tag{2}$$

where L is the distance between two bonded atoms, L_0 is the experimental bond length (2.27 Å), and α is the strength of the potential as determined by Lucovsky. The second term is also harmonic and relates to the angle between the bonds on a given atom. This term has the form

$$U_{\text{bend}} = (\tfrac{1}{2})\beta(\theta - \theta_0)^2 L_0^2 \ , \tag{3}$$

where θ is the angle between two bonds, θ_0 is the experimental bond angle, and β is the strength of the potential. The constants θ and β have different values for the two type of atoms.

The latter two terms of the potential of Eq. (1) are based on the quadrupole of charge created by the lone-pair (LP) electrons on the sulfur atoms. The quadrupole can be modeled as two negative charges projecting out from the nucleus of the sulfur which is assigned a charge of $+2$ for the sake of charge conservation. For the interaction of these quadrupoles on two sulfur atoms, we defined the last two terms of the potential as the "crossing" and "pointing" terms. For the crossing term we assigned a vector to each of the sulfur atoms which points from the nucleus to one of the negative charges. The angle between these two vectors, ϕ_{cr}, has an optimal value of 90°, which represents the two vectors being crossed [Fig. 2(a)]. For the pointing term, we define two vectors on the sulfur atom being relaxed. The first points from the nucleus to the negative charge. The second points from the center of the atom to the other atom [Fig. 2(b)]. The angle between these two vectors, ϕ_{pt}, also has an optimum value of 90°, and thereby avoids having the charges on one *sulfur* pointing toward the other sulfur. The potentials for each of these two terms are harmonic with an additional weighting term $\exp(-\gamma r/r_0)$ included to define the effective range of interaction. The crossing term is

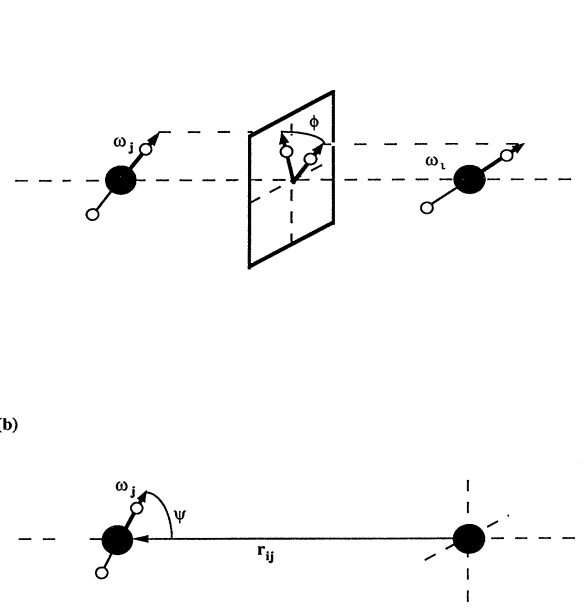

FIG. 2. (a) The angle used in the crossing term of the potential. (b) The angle used in the pointing term of the potential.

$$U_{LP\text{-cross}} = \tfrac{1}{2} K_{\text{cr}} \left[\phi_{\text{cr}} - \frac{\pi}{2} \right]^2 \left[\frac{e^{-\gamma r}}{r} \right], \tag{4}$$

and the pointing term is

$$U_{LP\text{-point}} = \tfrac{1}{2} K_{\text{pt}} \left[\phi_{\text{pt}} - \frac{\pi}{2} \right]^2 \left[\frac{e^{-\gamma r}}{r} \right], \tag{5}$$

where r is the distance between the two sulfur atoms. K_{cr} and K_{pt} were determined through the calculation of the bulk modulus of one of the models. The value of γ was chosen to allow strong interaction between second nearest-neighbor sulfur atoms.[25]

Most of the bonds in the model are created by bonding additional atoms to the existing portion of the model. Other bonds, between existing atoms, must be created during model growth to avoid dendritic growth. To create these other bonds, a building correction potential is used. This potential represents an attractive force between heteropolar atoms with unfulfilled bonds. The potential has a $1/r$ form which represents a Coulombic attraction between the two atoms. Once two atoms are within a reasonable distance, a trial bond is made and tested. If the bond lengths and angles resulting from the trial bond are within a certain tolerance of their anticipated values, the bond becomes permanent. One of the major difficulties that had to be overcome in this program was building the models with the correct density. To solve this problem, a density-correction potential was created. Once the model exceeded the radius at which the radial distribution function becomes washed out (about 7.5 Å), all additional atoms were placed subject to this potential. The anticipated radius of an additional atom was calculated based on the current mass of the model and the known value of the density. The atom was then given a potential of the form $(r - r_0)^4$, where r_0 is the calculated radius and r is the actual radius of the atom from the center of the model. The r^4 potential allows a small amount of deviation from the expected radius, but large deviations are avoided. During growth, another correction potential was used to avoid the creation of "bad pairs" of atoms. In reality, the existence of a bad pair would result in the creation of an additional bond between the two atoms while other bonds were broken. Our simple program does not allow for the breaking of bonds, so we used a "hard-sphere" potential to avoid the creation of bad pairs. A bad pair is a bonded pair of atoms initially grown into the sample in a configuration such that their separation is less than the equilibrium bond distance. It should be stressed that this is a potential term used during model growth. Clearly once an atom has bonded, relaxation can result in a distribution of nearest-neighbor separations, including whose with separations less than the most likely value (i.e., the value at the first peak of the radial distribution function). This hard-sphere growth potential is quite simple. If the atoms are far enough apart, then the potential vanishes. If the atoms are within a bond length, however, the potential is effectively infinite, thus forcing the atoms into any configuration which avoids the bad-pair configuration.

C. Accuracy of the model

A model of 1790 atoms was built according to the above method over a period of 9 days on a DEC MicroVax. In comparing the model to experiments done on the actual material, one must distinguish between explicit comparisons that can be made after the model is built, and implicit comparisons that are incorporated into the construction of the model itself. Explicit comparisons between our model and real data include: radial distribution functions; x-ray and neutron scattering spectra; and pair distribution functions determined from XAS experiments. Implicit comparisons include the sample density, infrared vibrational frequencies, and bulk moduli. We discuss each of these comparisons separately below.

Implicit inclusion of bond strengths through use of infrared vibrational data presumes that the structure of the model and that of the actual material are similar. Since all other comparisons of the model and the actual material show striking similarities, it is reasonable to use the potential strengths (α and β) that were determined from ir results.[12] The model also agrees implicitly with the experimental bulk modulus because the constants K_{cr} and K_{pt} were determined from these values. A final implicit agreement lies in the density of the model which was adjusted by controlling the As—S bond length and devising a growth algorithm that avoided dendritic growth. Insofar as all of these implicit agreements are built into the model during construction, the "agreement" between the model and the actual material is self-fulfilled. More meaningful comparisons involve explicit independent observations made after construction of the model. Table I lists major data concerning the model. The values for

TABLE I. Major data concerning the model.

Model parameters
$L_0 = 2.27$ Å
$\theta_{As} = 100.9°$
$\theta_S = 101.3°$
$\gamma = 1.006$ Å^{-1}
$\alpha = 8.67$ eV/Å^2
$\beta_{As} = 2.00$ eV/Å^2
$\beta_S = 2.81$ eV/Å^2
$K_{cr} = K_{pt} = 0.316$ eV/Å
$\phi_{cr} = \phi_{pt} = 90°$
Model Statistics
Number of atoms = 1790
Calculation time ≅ 3 CPU days on a Micro-Vax
Average bond length = 2.298 Å (2.27 Å)
Average As bond angle = 103.03° (100.9°)
Average S bond angle = 102.61° (101.3°)
Average density = 3.112 g/cm^3 (3.187 g/cm^3)

averages bond length, bond angles, and density are in close agreement with the experimental values shown in parentheses in the table.

Perhaps the most critical experimental comparison that can be appealed to in discussing the accuracy of the model lies in its agreement with the pair distribution functions determined from x-ray absorption spectroscopy, or XAS. The XAS data allow three direct experimental comparisons of pair distribution functions. The As-S first-nearest neighbor (and thus the S-As neighbor) is measured to be at 2.28±0.01 Å in the actual material and 2.3±0.1 in the model. The As-As second-nearest neighbor is measured to be 3.52±0.01 Å in the actual material and 3.5±0.1 in the model. Within the accuracy of the XAFS experiment and the spread of bond lengths in the model, it can be said that for these pairs the agreement is excellent.

Although we have not measured the XAFS at the sulfur edge we can make some statements from EXAFS data and topological constraints about the S-S second-nearest-neighbor pair-distribution function in the actual material. As shown above, the first-nearest-neighbor As-S distance is measured to be identical for the crystalline and amorphous material. It has been shown in other XAS work[3] that the S-As-S angle is—within experimental error—the same in the amorphous material as in the crystal. From this information and the density of the amorphous material we can conclude that the As-S-As angle must not deviate by more than approximately one degree from the crystalline value. This allows us to determine the S-S second nearest-neighbor distance in the actual material to be 3.5±0.1 Å, which is identical to the value and spread measured in our model.

The use of XAFS experimental results thus allows us to make explicit comparisons of atomic pair distances, and all suggest that within the experimental accuracy our model replicates the actual material. The As-S (and thus the S-As) first-nearest-neighbor distance is 2.28±0.01 Å (versus 2.3±0.1 Å in the model). The As-As second-nearest-neighbor distance is 3.52±0.01 Å (versus 3.5±0.1 Å in the model). And both the model and the XAFS results give as the S-S second-nearest-neighbor distance 3.5±0.1 Å This study of pair distribution functions and interatomic distances clearly underscores several strengths of XAFS techniques. The atom-specific nature of XAFS allows one to focus on particular environments, and the use of the phase-corrected Fourier transform[4] allows clear separation of atomic species in any given shell surrounding the chosen environment. Comparison of specific pairs in the actual material to those in the model is thus made experimentally possible. And the agreement is excellent.

It is important to remember that these comparisons are of *pair* distribution functions involving explicit pairs. This is in contrast to *radial* distribution functions which do not distinguish between the atomic identity of pairs. Both XAFS and structural modeling allow comparison of explicit pairs while the measurement and calculations of radial distribution functions does not. The ability to separate individual contributions within one shell in x-ray absorption spectroscopy requires a clear phase difference between species one is trying to resolve.[4] In the case of As and S, the scattering-phase difference is nearly 90°, which is the ideal phase difference for resolving separate components with a shell. Of course the comparison of distinct pair distribution functions is not possible in models of elemental solids.

Other explicit experimental results that the model can be compared with include the radial distribution function and x-ray (and neutron) diffraction intensity, $I(k)$. These can be calculated from the model. The calculations for both the radial distribution function and $I(k)$ are shown in Appendix B.

An examination of the radial distribution function (as shown in Fig. 3) for one sample of the actual material[26] and for the model allows one to compare both bond

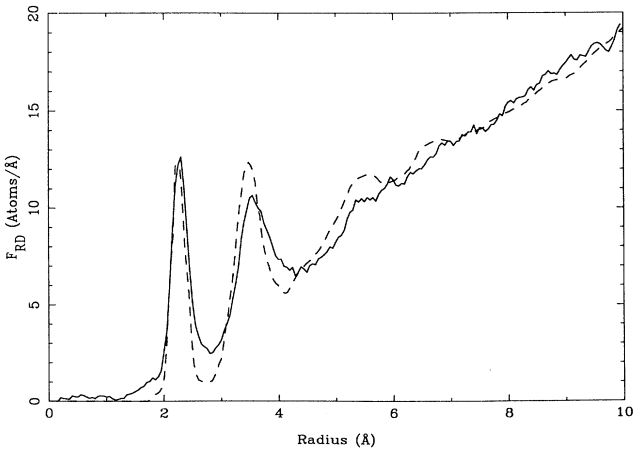

FIG. 3. The radial distribution functions (F_{RD}) for the model (solid line) compared with experimental results of Ref. 18 (dashed line).

lengths and density. The first peak in the F_{RD} corresponds to the bond length between atoms and it is where it should be at about 2.27 Å. The second peak is at about 3.5 Å and corresponds to the second-nearest-neighbor pairing. Although peak widths can vary slightly from sample to sample, the positions vary only slightly. Comparison of experimental F_{RD}'s with the model should be made keeping in mind the fact that the experimental F_{RD}'s can differ slightly in peak width[3,26] so that exact replication of widths in the model is not critically important. Also important in the comparison of the model and the material as shown in Fig. 3 is the comparison of the overall curvature of the background. The fact that the model curvature replicates that of the actual material reflects and accurate and uniform density in the model. Preliminary versions of the model-building program did not incorporate algorithms for avoiding dendritic growth and other structures that would result in nonuniform and inaccurate densities.[27] The final version of our model-building program as described in the previous section included an algorithm that resulted in the good agreement shown in the large-r portion of Fig. 3. It is important to choose an F_{RD} that extends cleanly to large-r values so that model density and topological uniformity can be compared. Our choice of experimental F_{RD} for comparison purposes was made with this in mind.

Figure 4 compares the experimental[28] and model $I(k)$. The model shows good agreement here as well with one minor exception. The model deviates from the experimental curve for k values below 2 $Å^{-1}$. This is to be expected since the low-k part of this spectrum depends upon very long-range correlations between atoms which are not present in our finite-sized model. The first peak in the $I(k)$ spectrum has been linked to intermediate-range order and the photodarkening effect,[18,26] and this peak has been fairly accurately reproduced with the present model. Thus, as far as this test is concerned, the model does not have intermediate-range order features incommensurate with the real material intermediate range order found in the model.

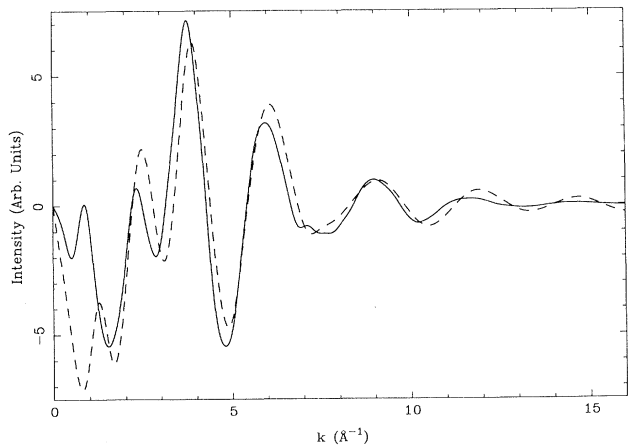

FIG. 4. The x-ray diffraction intensity $I(k)$ for the model (solid line) compared with experimental results of Ref. 19 (dashed line).

It is important to put the present work in proper perspective with respect to earlier modeling studies. In general, it can be said that most models involve implicit inclusion of vibrational data (through inclusion of bound strengths and a presumption about general model structure) and the density (through inclusion of proper bond length). It has likewise been the case in most modeling studies that comparison with radial distribution functions has been made and that such comparisons are often favorable. The present study includes all of these features, but it goes considerably further in its contact with experimental data in several ways. First, the bulk modulus is implicitly included. Second, comparison with neutron and x-ray diffraction spectra is direct and favorable. Finally, a comparison of four distinct pair distribution functions is explicitly made, and the comparison is quite good.

D. Structure in the model

Intermediate-range order is not well defined in the x-ray diffraction results or in the radial distribution function. In a model one has in hand, however,

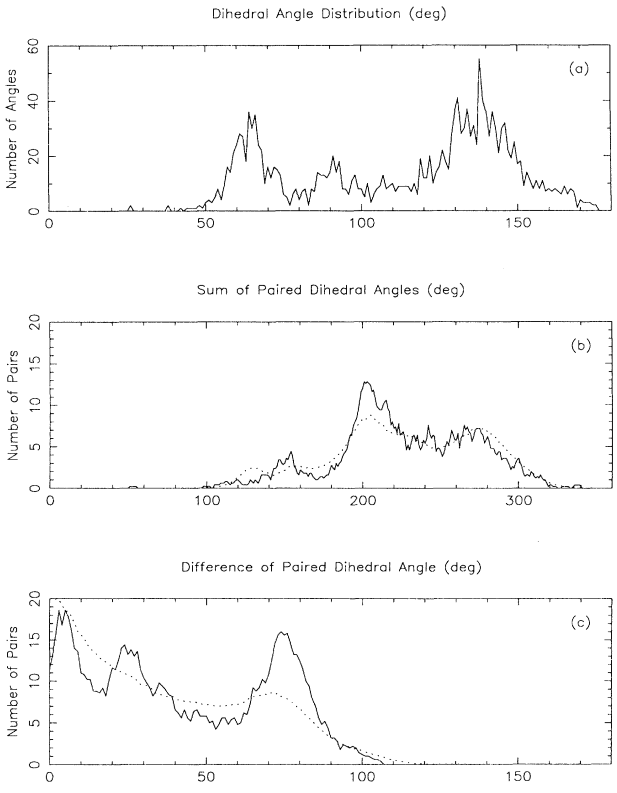

FIG. 5. (a) Dihedral angle distribution plot. (b) Distribution of the sum of paired dihedral angles (solid line) compared with random pairing (dotted line). (c) Distribution of the difference of paired dihedral angles (solid line) compared with random pairing (dotted line).

intermediate-range order that can be examined in some detail. Thus, insofar as we have developed a model which agrees quite well in experiment with the real material, it is of interest to investigate the intermediate-range order in our model.

In order to describe the intermediate-range order in the model, one must consider the relationships between pairs of dihedral angles. To define a dihedral angle, we first describe the orientation of an atom in terms of a vector which is the sum of the bond vectors connecting it with its first nearest neighbors. A dihedral angle can then be defined as the angle between the orientation vectors on two neighboring atoms. If one considers a sulfur atom which connects two AsS_3 pyramids, we have a pair of dihedral angles on each sulfur atom which describes the orientation of the adjacent A_2S_3 pyramids. Luedtke and co-workers[22] describe the correlation between pairs of dihedral angles using distribution functions describing the average sum and average difference between the two dihedral angles in each pair. Any variation between these functions and similar functions calculated for random pairing provides evidence for IRO in the model.

Another method which we used in our previous work[7] is to create a scatter plot on which each S atom is assigned on point representing its local environment. The coordinates on such a plot can be the atom's two dihedral angles with the greater angle being defined as the ordinate. Such a plot can be examined for clustering which would be indication of a preferred order in the model. On a scatter plot for a crystalline sample, only two S environments would be found: one representing the helical S environment and one representing the bridging S atom between two helices. In an amorphous model, any clustering in these regions would suggest the existence of the structures which give rise to these environments in the crystal.

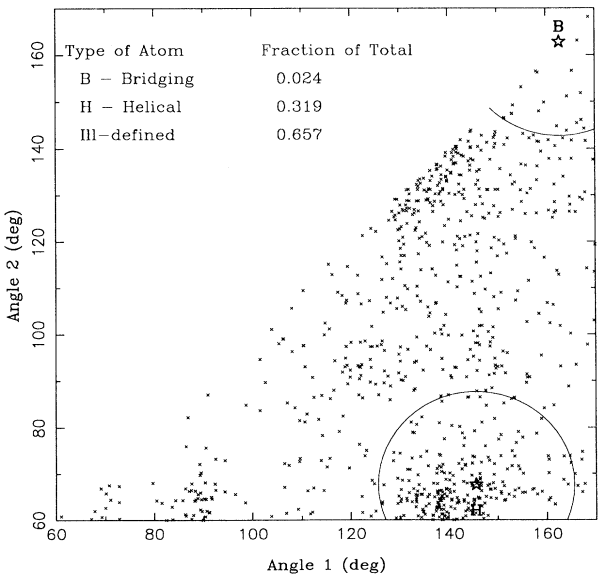

FIG. 6. Scatter plot of dihedral angle pairs in the model. The greater of the angles is plotted as the abscissa. Points *B* and *H* show the bridging and helical sulfur sites from the crystal.

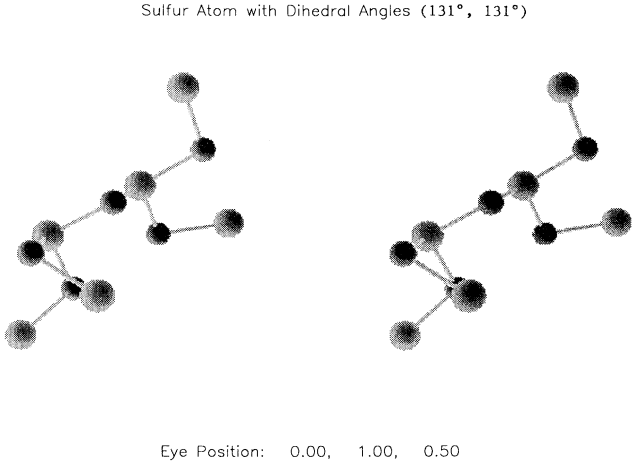

FIG. 7. Stereoscopic computer drawing of a sulfur atom with dihedral angle (131°, 131°). Sulfur atoms are smaller and darker than arsenic atoms.

Evidence for intermediate-range order in the model is seen in these two dihedral angle plots. In the angle distribution plots (Fig. 5) we have a noticeable variation from the random-pairing graph. In the scatter plot (Fig. 6) we have noticeable clustering in at least two places. The sum distribution plot shows a peak which is higher than it would be for random pairing at about 200 degrees. This corresponds to the peak in the difference graph at 75 degrees and to the clustering shown on the scatter plot at (140°, 65°). The scatter plot shows that these pairs lie in the region near the helical S-atom site from *c*-As_2S_3. From this we conclude that the helical form which is found in the amor-

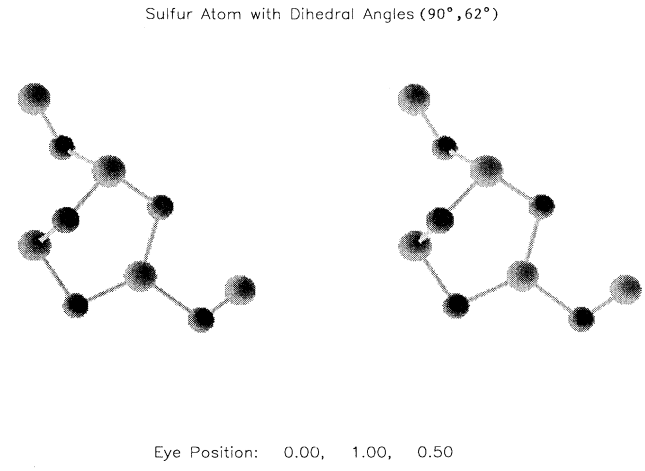

FIG. 8. Stereoscopic computer drawing of a sulfur atom with dihedral angles (90°, 62°). Sulfur atoms are smaller and darker than arsenic atoms.

phous state represented by our model.

There is also some clustering on the scatter plot between (130°, 130°) and (150°, 105°). These points correspond to the range of 260°–300° on the sum plot and 0° on the difference plot. Notice that the graphs at these points are close to the graph for a random pairing, which means that this particular pairing occurs as a random event rather than as a preferred pair configuration. This suggests that these neighborhoods are an artifact of a single preferred dihedral angle, i.e., a shorter-range ordering. Nevertheless, this configuration could represent a sulfur atom bridge between two crossing helices, as suggested by the computer picture for the pair (131°, 131°) shown in Fig. 7. There is a small peak of the sum graph at 150° which corresponds to the peak at 25 degrees on the difference graph. These peaks correspond to a minimal amount of clustering on the scatter plot in the area (85°, 65°). The computer picture for the pair (90°, 62°) (Fig. 8) shows that this pairing occurs in the six-membered ring configuration. Such six-membered rings can be formed at the termination point on two intersecting helices.

The scatter plot shows a distinctly low number of sulfur atoms in the neighborhood of the bridging sulfur site. Since bridging sulfur atoms form the chains into planar structures, this suggests that this model does not contain such planes. Furthermore, no other clustering is evident, so we have seen no evidence for the existence of bridged parallel chains in the model.

Insofar as the present model is an accurate depiction of reality, one can say the following: that a-As_2S_3 contains helical units which are linked together by bridging sulfur atoms as found in the crystal. Unlike the crystal, however, the helical axes are not parallel, so the bridging sulfurs are randomly twisted. The existence of six-membered rings is not incompatible with the model, but no evidence for planar or bridged-like structures are evident.

IV. CONCLUSIONS

A model of a-As_2S_3 has been constructed in a computer that has avoided or minimized many of the shortcomings of previous models. In particular the model: (i) agrees substantially with all experimental checks that can be made on it and on the real material; (ii) avoids building biases inherent in models constructed by hand-built means or by adapting models of similar materials; (iii) is appreciably larger than other finite-size models, thus diminishing the effect of the surface; (iv) does not depend on periodic boundary conditions; (v) includes subtleties in its bonding potential that are known to determine structure in the crystalline counterpart; and (vi) is constructed with considerable economy in use of computer time.

A study of dihedral angle statistics in the model suggests that intermediate-range order in a-As_2S_3 may best be characterized in terms of small helical segments comprised of linked AsS_3 pyramids. In addition there is evidence for the existence of six-membered rings that form the termination of two intersecting helical chains. There is no suggestion in the model of planar or bridged-like structures.

Currently underway are efforts to develop further the modeling techniques used in the present study. A bond-switching mechanism is being incorporated into the growth process to relieve built-in stress. The program is being made more efficient to allow growth of larger models so as to further minimize the effect of the surface and more carefully compare the model to observed x-ray diffraction data taken on the real material.

ACKNOWLEDGMENTS

This work was supported in part by NSF Grants Nos. DMR8803370 and DMR8904386. I would like to thank Michael Paesler for his guidance and helpful suggestions as well as for a critical reading of the manuscript.

APPENDIX A

The model-building process is outlined in the flow diagram of Fig. 9. The program begins by reading any previous data that were left the last time the program was run. A model is begun with an AsS_3 pyramid which is used as a seen. Next, the program finds the neighbors of all existing atoms. The neighbors of a given atom are all atoms within 5 Å of that atom. These neighbors are used in the calculation of the lone-pair potentials and in the building and bad-pair correction potentials. Next the program adds additional atoms to the model five atoms at a time. For each atom, it finds the innermost atom of the model which has unfulfilled bonds. It then attached an

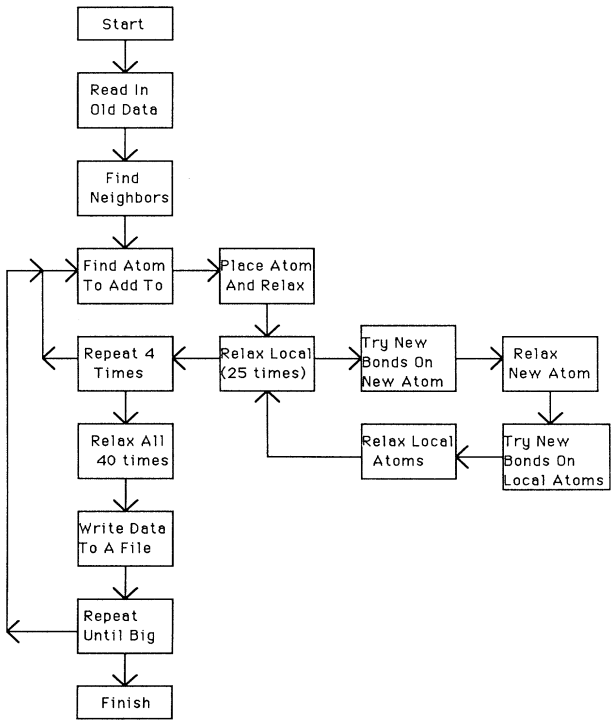

FIG. 9. Flow diagram of the modeling process.

additional atom, places it at a random position, relaxes it into place, and determines its neighbors. Next the program performs a local relaxation where the local structure is defined as the neighbors of the additional atom. For each relaxation step, the program attempts to form additional bonds within the local structure and performs a relaxation on each of the local atoms. This process is repeated for 25 relaxation steps. The entire placement and local relaxation process is repeated for each of the five additional atoms. After adding the additional atoms, the program relaxes all atoms in the model 40 times. This allows any additionally introduced stress to be removed from the model before more atoms are added. The program writes the model to a file after every global relaxation. This allows one to monitor its progress and it minimizes losses in the event of a computer crash. This entire process can be repeated until the model is as large as one wants. The relaxation process used on all the atoms involves randomly moving the atoms to lower energy positions as determined by our potential equations. We use the four-part potential and the correction potentials described in the text.

APPENDIX B

The radial distribution function F_{RD} describes the density of the model as a function of distance from any atom. This is calculated by tallying up the number of pairs in the model which are a certain distance apart. This sum, taken for all possible distances is the radial distribution function. This sum is given by the equation

$$F_{\mathrm{RD}}(r)=\sum_{i}\sum_{j\neq 1} W(r_{ij}) .$$

For an infinite model, the function $W(r_{ij})$ is unity for all values r_{ij}. Since models are finite, one must use a weighting function which takes the size of the model into account. The function employed in the present study is given by

$$\frac{1}{W(r)}=1-\frac{3}{4}\left[\frac{r}{r_m}\right]+\frac{1}{16}\left[\frac{r}{r_m}\right]^3$$

which is the equation for the volume enclosed by two overlapping spheres of radius r_m with distance r between the centers. This function gives extra weight to longer pairs in the model which occur less frequently than they would if the model extended infinitely.

As expected, the radial distribution functions derived in this manner are quite accurate for low-r values, but tend to display unrealistic features of r values greater than the radius of the model. For this reason, for further calculations and for comparison to experimental results the F_{RD} out to one model radius only was used.

The calculation of the x-ray diffraction intensity $I(k)$ is simply a transform of pair distribution functions to k space. The pair distribution function $G(r)$ is calculated by subtracting the radial distribution function for a homogeneous sphere from the radial distribution curve, i.e.,

$$G(r)=F_{\mathrm{RD}}(r)-\rho_0(\tfrac{4}{3}\pi r^3) .$$

Given the pair distribution function, the x-ray-diffraction intensity is given by

$$I(k)=\int_0^\infty \frac{f^2 G(r)\sin(kr)}{kr}dr ,$$

where f is the scattering factor of the material.

Since arsenic sulfide consists of two elements with different scattering factors, one must expand upon this definition. The pair distribution function must be split into four possible atomic pairings, As-As, As-S, S-As, and S-S. Using the partial pair distributions $G_{mn}(r)$ and the individual scattering factors f_m and f_n, Eq. (4) becomes

$$I(k)=\sum_m\sum_n\int_0^\infty \frac{f_m f_n G_{mn}(r)\sin(kr)}{kr} .$$

Finally, the scattering intensity is multiplied by an $e^{-\alpha r}$ factor to simulate the decay of the function found in experimental data.

[1]J. C. Phillips, Phys. Today **35**, 27 (1987).

[2]N. Shevchik, Ph.D. thesis, Harvard University, 1972.

[3]C. Y. Yang, M. A. Paesler, and D. E. Sayers, Phys. Rev. B **36**, 9160 (1987); C. Y. Yang, Ph.D. thesis, North Carolina State University, 1987.

[4]D. C. Koninsberger and R. Prins, *X-Ray Absorption* (Wiley, New York, 1988), Chap. 6.

[5]G. Lucovsky and Richard M. Martin, J. Non-Cryst. Solids **8/9**, 185 (1972).

[6]A. P. DeFonzo and J. Tauc, Phys. Rev. B **18**, 6957 (1978); P. C. Taylor, S. G. Bishop, D. L. Mitchell, and D. Treacy, *Proceedings of the Vth International Conference on Amorphous and Liquid Semiconductors, Garmisch* (Taylor and Francis, London, 1974), p. 1267; L. E. Busse, Phys. Rev. B **26**, 3639 (1984).

[7]G. Pfeiffer, C. J. Brabec, S. R. Jefferys, and M. A. Paesler, Phys. Rev. B **39**, 12 861 (1989); B. T. Kolomiets and V. P. Pozdnev, Fiz. Tverd. Tela (Leningrad) **2**, 28 (1960) [Sov. Phys. Solid State **2**, 23 (1960)]; R. Zallen, R. E. Drews, R. L. Emerald, and M. L. Slade, Phys. Rev. Lett. **26**, 1564 (1971).

[8]M. Rubenstein and P. C. Taylor, Phys. Rev. Lett. **29**, 119 (1972); Phys. Rev. B **9**, 4258 (1974).

[9]J. C. Phillips, C. A. Beevers, and S. E. B. Gould, Phys. Rev. B **21**, 5724 (1980).

[10]W. J. Bresser, P. Boolchand, P. Suranyi, and J. P. de Neufville, Phys. Rev. Lett. **46**, 1689 (1981).

[11]M. F. Daniel, A. J. Leadbetter, A. C. Wright, and A. N. Sinclair, J. Non-Cryst. Solids **32**, 271 (1979).

[12]S. R. Elliott, J. Non-Cryst. Solids **97/98**, 159 (1987).

[13]Jeffrey S. Lannin, J. Non-Cryst. Solids **97/98**, 203 (1987).

[14]David L. Price, Sherman Susman, and Adrian C. Wright, J. Non-Cryst. Solids **97/98**, 167 (1987).

[15]G. Lucovsky, R. J. Nemanich, S. A. Solin, and R. C. Keezer,

Solid State Commun. **17**, 1567 (1975).
[16]D. Gerlich, E. Litov, and O. L. Anderson, Phys. Rev. B **20**, 2529 (1979).
[17]S. R. Elliott, *Physics of Amorphous Materials* (Longmans, New York, 1984), pp. 94–103.
[18]T. G. Fowler and S. R. Elliot, J. Non-Cryst. Solids **92**, 31 (1987).
[19]T. Fujiwara, S. Itoh, and M. Okazaki, J. Non-Cryst. Solids **45**, 371 (1981).
[20]L. F. Gladden and S. R. Elliot, J. Non-Cryst. Solids **97&98**, 383 (1987).
[21]M. D. Rechtin, A. L. Renninger, and B. L. Averbach, J. Non-Cryst. Solids **15**, 74 (1974).
[22]W. D. Luedtke and U. Landman, Phys. Rev. B **40**, 1164 (1989).
[23]F. Wooten and D. Weair, J. Non-Cryst. Solids **97&98**, 349 (1987).
[24]Radu Grigorovici, Paul Gartner, and Ion Corcotoi, J. Non-Cryst. Solids **114**, 256 (1989).
[25]J. M. Lee (private communication).
[26]M. F. Daniel, A. J. Leadbetter, A. C. Wright, and A. N. Sinclair, J. Non-Cryst. Solids **32**, 271 (1979).
[27]Problems with internal connectivity—one type of which manifests itself as dendritic growth—are discussed in Ref. 17.
[28]K. Tanaka, Appl. Phys. Lett. **26**, 243 (1975).